Supplementary Information

Supplementary Figures

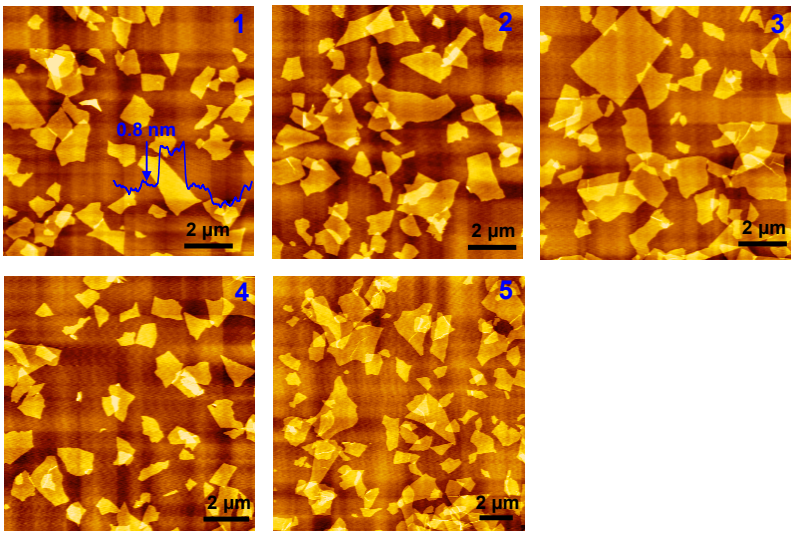

Supplementary Figure S1|AFM images of GO sheets in tapping mode. The width distribution *P(w)* of GO sheets is counted and calculated from images 1-5. We defined that the irregular sheets are regarded as squares of the equal area and the diameter of sheets as the side length of squares. The relative standard deviation (σ_w) is calculated according to $\sigma_w = (\langle W^2 \rangle - \langle W \rangle^2)/\langle W \rangle$.

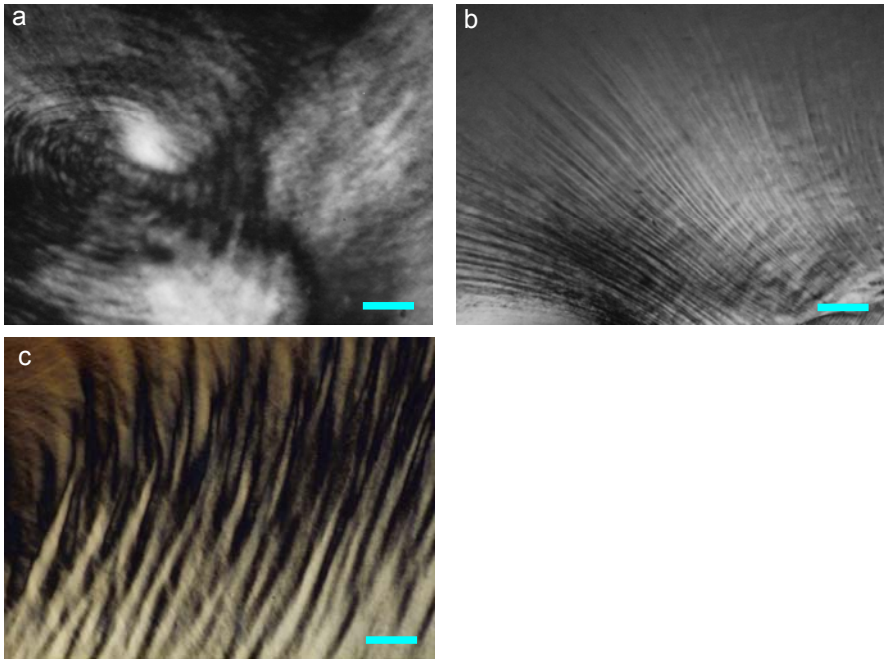

Supplementary Figure S2|Fingerprint-like optical textures of GO CLCs. a: focal conic texture with fingerprint features. b,c: fingerprint textures. Scale bars 200 μm. All the figures are captured between crossed polarized light.

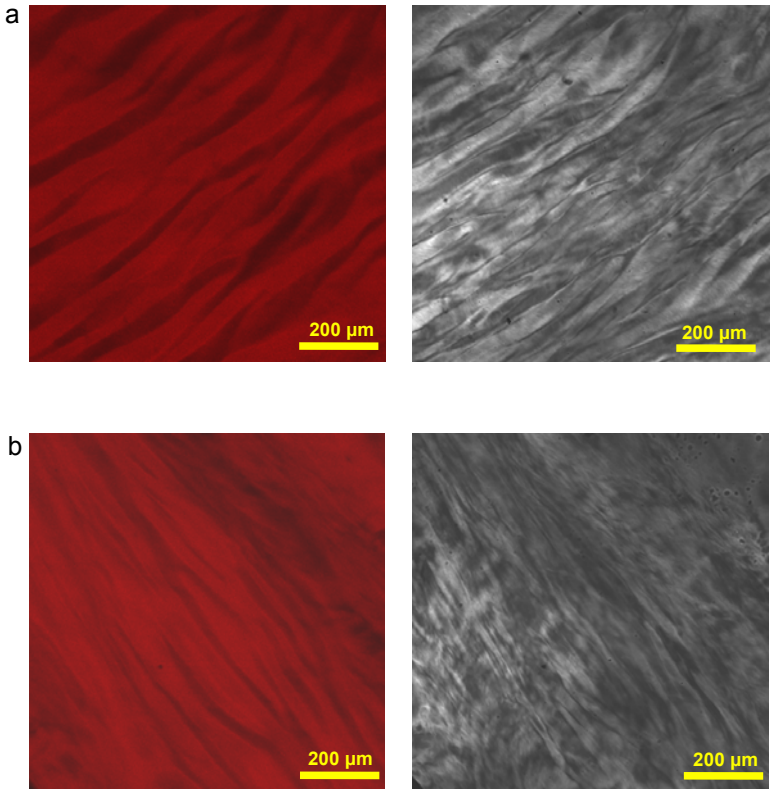

Supplementary Figure S3|Fluorescence confocal images of the band-like fingerprint textures.

The volume fraction (ϕ) of the sample is 0.78 %. The left images are the fluorescent images and the right ones are the bright field images.

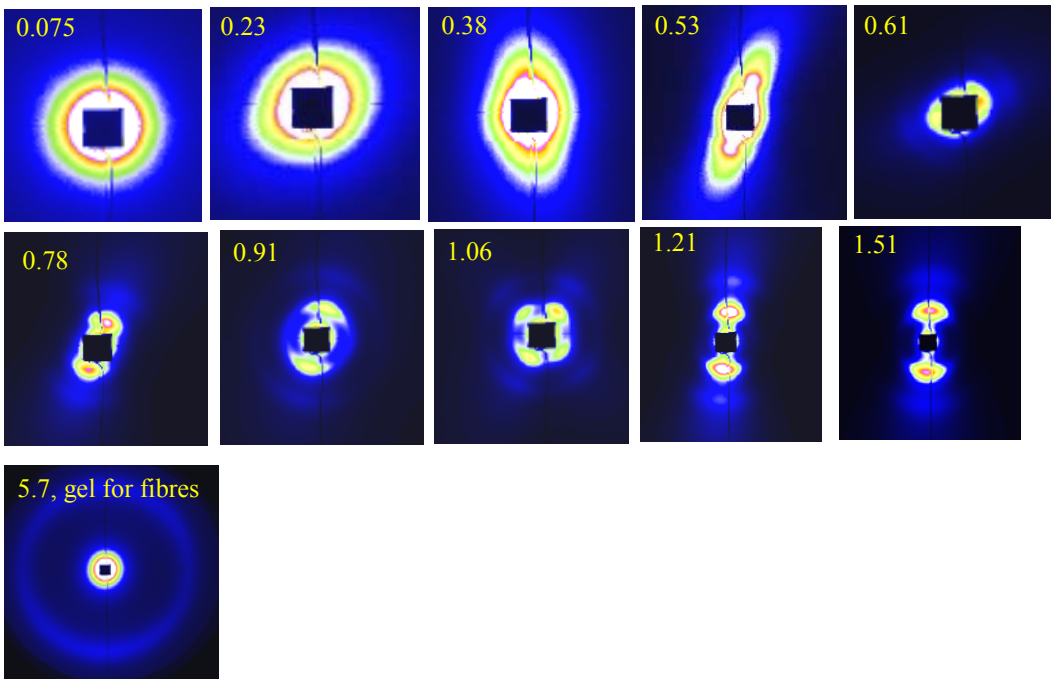

Supplementary Figure S4|SAXS 2D patterns of GO CLCs depending on concentrations. The numbers labeled on the pattern are the corresponding concentrations ϕs (%). The last pattern was obtained from the sample with ϕ 5.7 %, which was used to spin neat GO fibres.

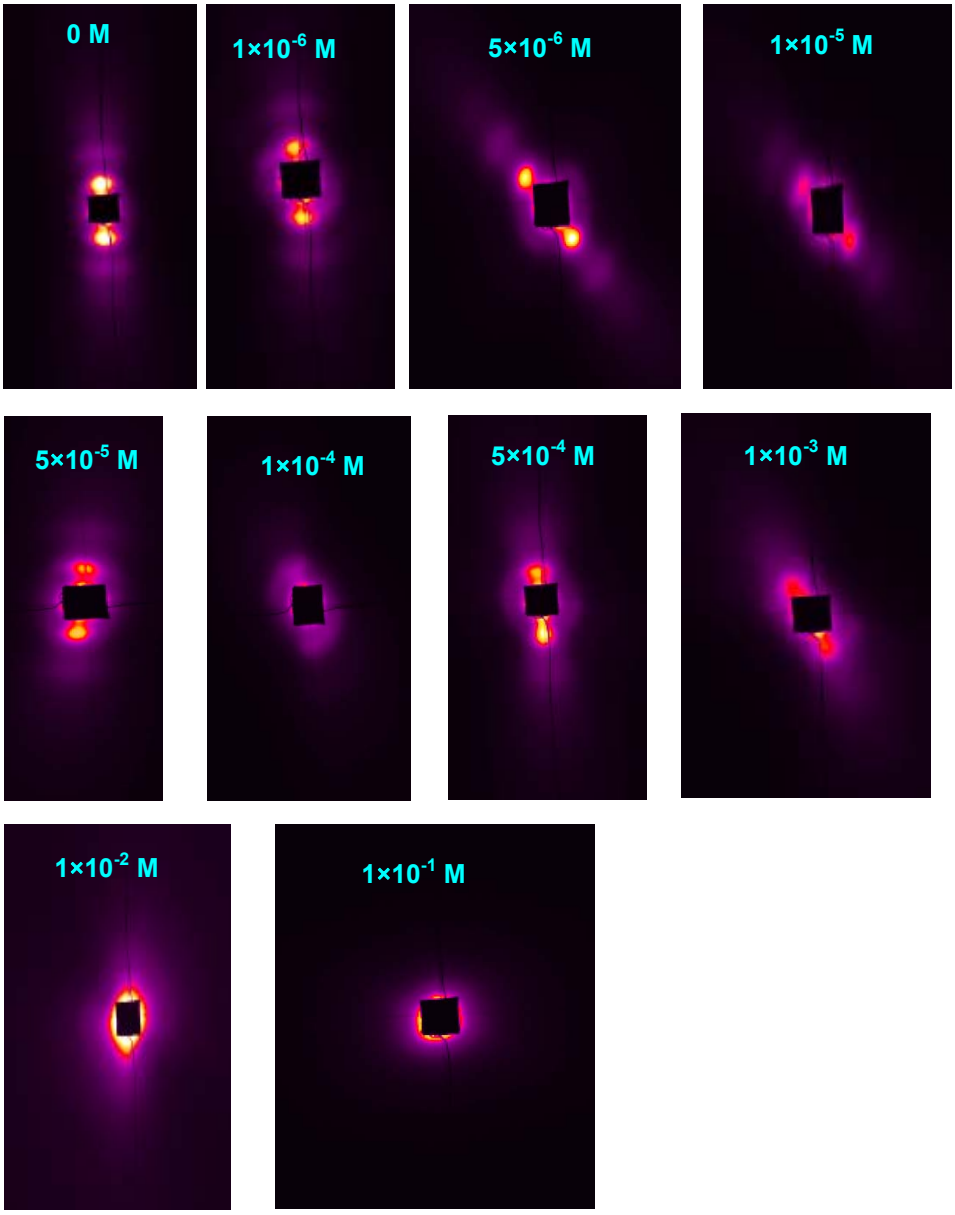

Supplementary Figure S5|SAXS patterns of GO CLCs (ϕ = 0.7 %) with gradient salt concentrations.

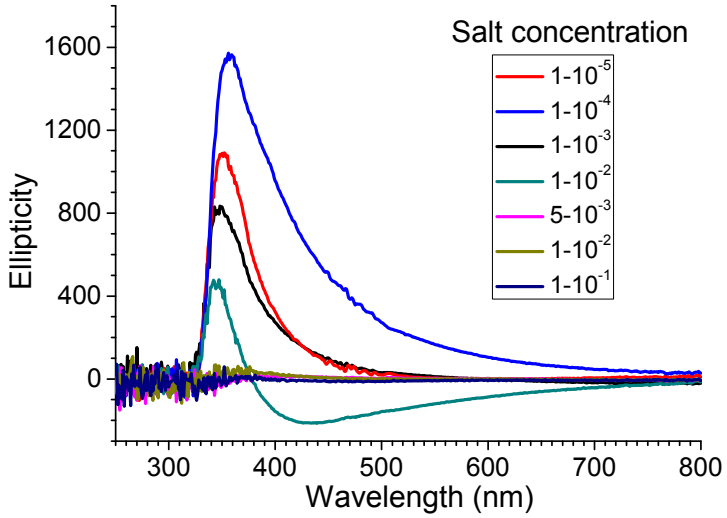

Supplementary Figure S6|CD spectra of GO CLCs with gradient NaCl concentrations.

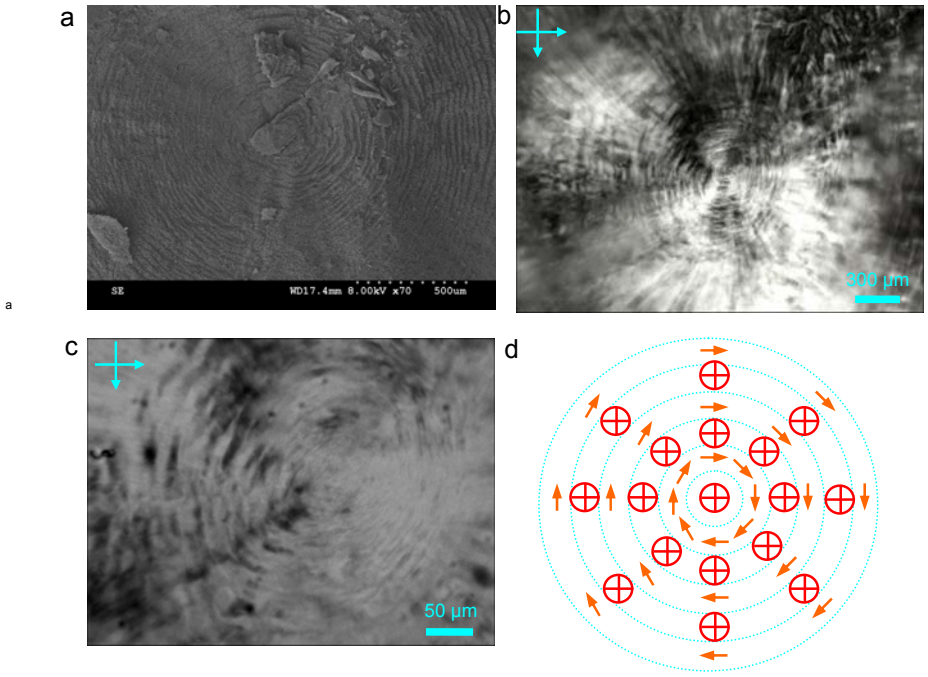

Supplementary Figure S7|a: Top view of Cryo-SEM image of GO CLC. b,c: the fingerprint optical textures of GO CLC with the same volume fraction in a. d: the corresponding vectors map of the fingerprint textures in b,c.

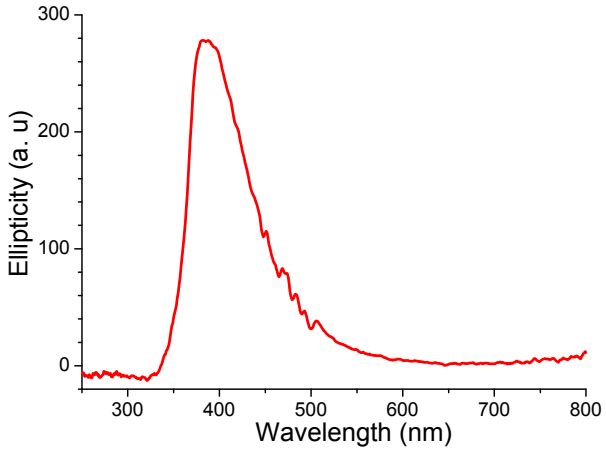

Supplementary Figure S8|CD spectrum of silica-based chiral gel film templating from the GO CLCs.

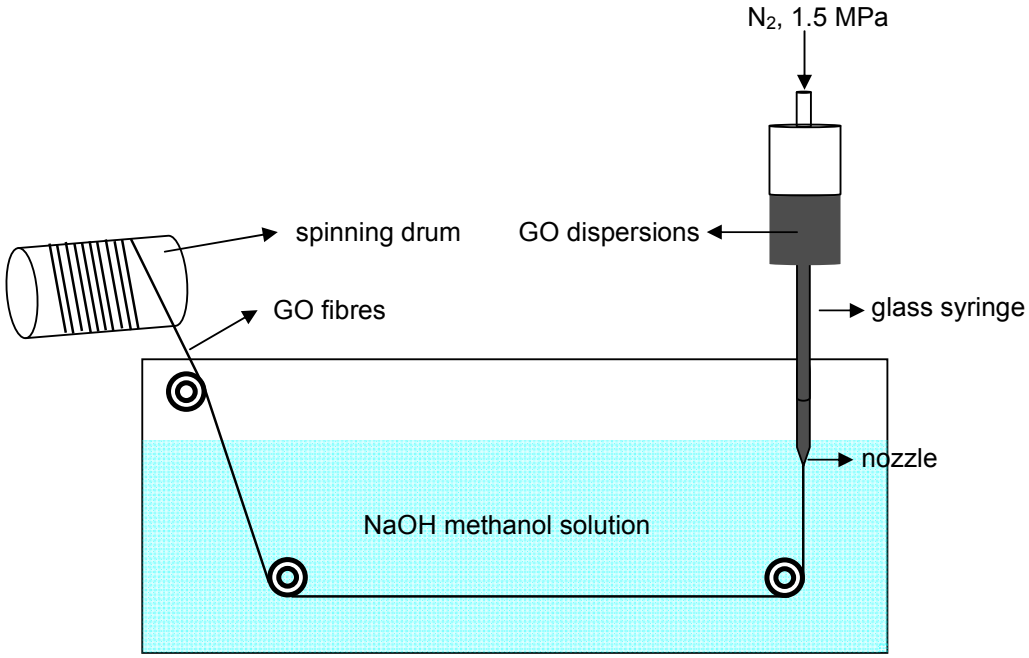

Supplementary Figure S9|Spinning apparatus for GO fibres from aqueous GO LCs.

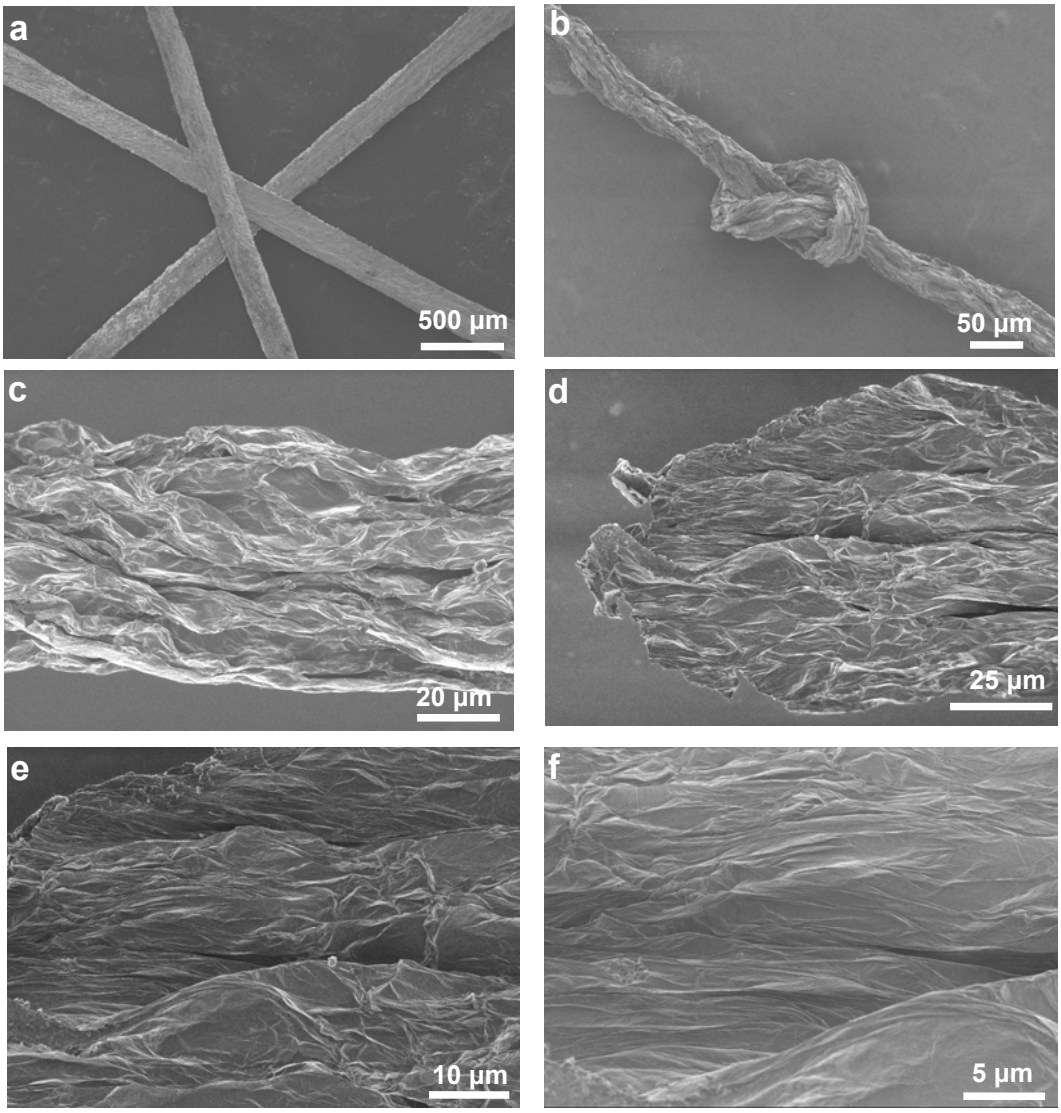

Supplementary Figure S10|SEM images of GO belts and fibres. a: SEM image of crossed GO belts spun from the GO dispersion (ϕ = 1.97 %). b: a tighten knot of GO fibre spun from GO LC (ϕ = 5.7 %). c: surface morphology of GO fibre. d-f: fracture morphology surface after tensile tests. The original crumbled surface of GO sheets gets stretched after tensile tests.

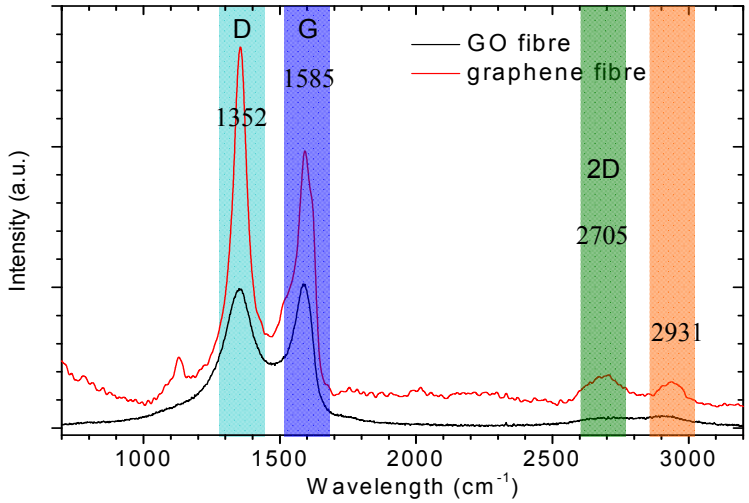

Supplementary Figure S11|Raman spectra of GO and graphene fibres. The integrated intensity ratio of D band (1352 cm^{-1}) to G band (1585 cm^{-1}) (I_D/I_G) decreases from 1.9 for GO fibre to 1.2 for graphene fibre, companying by the emergence of the 2D band (2705 cm^{-1}), showing less sp^3 carbon defects, *i.e.* more sp^2 carbon for graphene fibres.

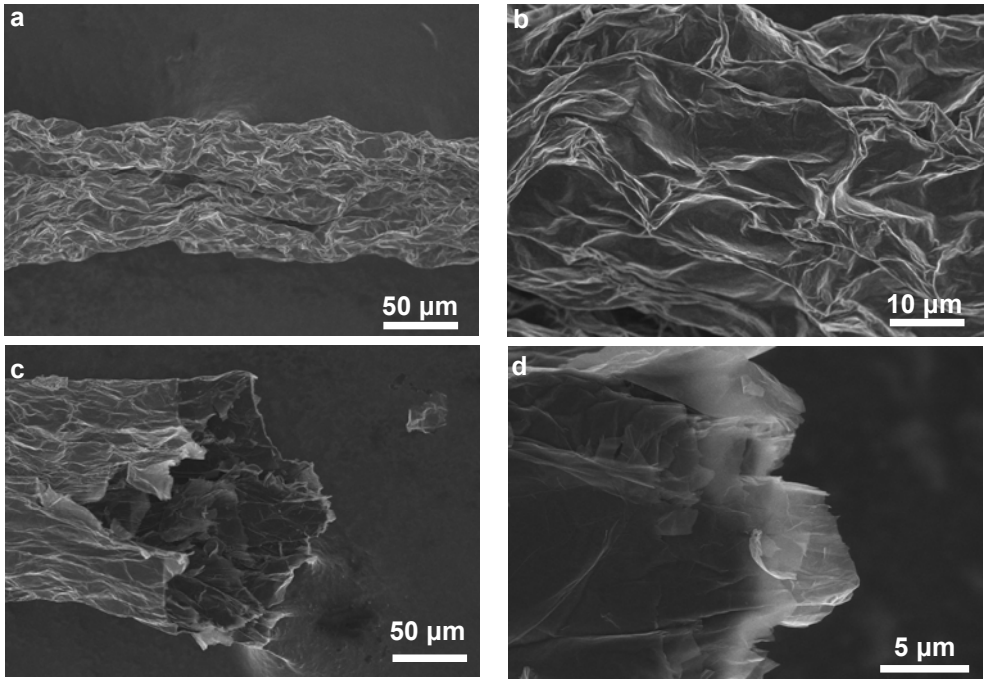

Supplementary Figure S12|SEM images of graphene fibres. a-b: SEM image of surface morphology of graphene fibre chemically reduced from GO fibre. c,d: fracture morphology of graphene fibre after tensile mechanical tests.

Supplementary Figure S13|Power law fit of X-ray scattering (q_0) at ϕ 2.12%.

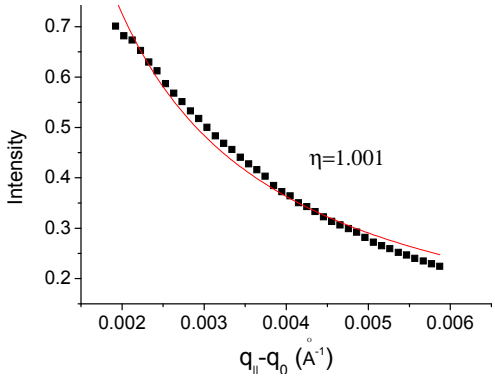

Supplementary Tables

Supplementary Table S1|SAXS data of chiral liquid crystal of GO.

ϕ (%)	0.23	0.38	0.53	0.61	0.76	0.91	1.06	1.21	1.51	2.12
q_0 (nm^{-1})	*	0.056	0.067	0.075	0.098	0.100	0.124	0.147	0.192	0.191
$2q_0$(nm^{-1})	*	0.112	0.139	0.155	0.203	0.209	0.253	0.298	0.393	0.389
$3q_0$(nm^{-1})	*	*	0.217	0.241	0.315	0.312	0.380	0.441	0.602	0.613
d_{001} (nm)	*	112.2	93.8	83.8	64.1	62.8	50.7	42.7	32.7	32.9

* No peak was detected.

Supplementary Table S2|Callié lineshape analysis results

ϕ (%)	0.38	0.53	0.61	0.76	0.91	1.06	1.21	1.51	2.12
q_0 (nm^{-1})	0.056	0.067	0.075	0.098	0.100	0.124	0.147	0.192	0.191
d_{001} (nm)	112.2	93.8	83.8	64.1	62.8	50.7	42.7	32.7	32.9
η	1.15± 0.04	1.26± 0.04	0.98± 0.03	0.90± 0.02	1.14± 0.03	1.12± 0.01	0.94± 0.03	1.25± 0.02	1.0± 0.02
B ($10^{-6}erg/cm^3$)	0.01± 0.002	0.02± 0.004	0.05± 0.01	0.19± 0.04	0.13± 0.03	0.31± 0.06	0.89± 0.2	1.46± 0.3	2.2±0.5
ξ (μm)	589.5± 93	516.8± 81.2	407.2± 63.8	368.5± 46	329.2± 52	263.4 ±41.6	203.2 ±31.8	179.4± 28.5	161.4± 25.7

Supplementary Note

Callié lineshape analysis. From Landau-Peierls instability in the system with the 1D density wave in 2D liquid medium and the P.G. de Gennes theory on the liquid crystals, the mean square fluctuations diverge logarithmically with the size of the sample[28]. Thus, the thermal fluctuation in smectic (lamellar) liquid crystals induced a quasi-long-range order, rather than the true-long-range order. In these LCs with layered structures, the positional correlation functions do not extend to infinity, but decay algebraically as some power of the distance[39]. This kind of algebraic decay of postional order has been experimentally observed in smectic liquid crystals. The mean-squared fluctuations $\langle u^2 \rangle$ in the longitudinal direction normal to the smectic layers can be calculated by the following equation:

$$\langle u^2 \rangle = (4\pi)^{-1}(BK)^{-1/2} k_B T \ln(q_{max} L/2\pi) \text{ for } \xi_M = 0$$

B : the bulk compression modulus

K: the elastic modulus

ξ_M: the magnetic coherence length.

k_B: the Boltzmann constant

In the powder sample, thermally induced layer displacements diverge logarithmically with the domain size and destroy the conventional long-range order, which causes the delta-functional Bragg peaks to be replaced by power law divergences. The consequence of the divergent real-space positional fluctuations for X-ray scattering is calculated in the harmonic approximation. On Fourier transforming for a sample to zero field, the X-ray scattering is predicted to follow

$$S(0, 0, q_{//}) \sim (q_{//} - q_0)^{-2+\eta_n} \qquad \eta_n \equiv q_z^2 k_B T/8\pi(BK)^{1/2}$$

The dimensionless parameter η determines the power-law line shape in the Callié continuum theory, and defined to be the value of η at the n_{th} order Bragg peak $q_z = n2\pi/d$. The parameter $\xi \equiv (kd/B)^{1/4}$, is a correlation length for the fluctuations. For distance greater than ξ, the height fluctuations are coherent from layer to layer while for distance less than ξ, fluctuations are single-layered and incoherent.

In conclusion, there are two important parameters (η and ξ) to describe the structural characteristics of LC samples in Callié line shape analysis[40-42]. The power exponent η can be obtained from the fitting of the SAXS profiles into power-law functions, and the correlation length ξ is readily extracted from:

$$\xi \equiv (kd/B)^{1/4} = (Kd^2/B)^{1/4} \qquad \text{(eq. S1)}$$

$$\eta_n \equiv q_z^2 k_B T/8\pi(BK)^{1/2} \qquad \text{(eq. S2)}$$

where T is the thermodynamic temperature (298 degree Kelvin), ξ the correlation length.

Before appling Callié line-shape analysis to the X-ray scattering of GO LC, we should get the compression modulus (B) between GO sheets intercalated by water molecules, or the elastic modulus of GO sheets (K). In GO liquid crystalline dispersions, GO sheets could be considered as suspending sheets. The curvature of GO sheets in LC brings a director splay distortion and the restoring force results in an elastic energy (K). The Young's modulus of single GO sheets has been obtained from the tip-induced deformation experiments on suspending GO sheets. Desipite the defect of GO sheets, the single sheets still exhibit extradinary stiffness with a Young's elastic modulus (E) of 0.25 Tpa[43]. As a result, the restoring force (K) on a single GO sheet can be calculated as:

$$K = E^{*}S_{GO,}\ S_{Go}\text{ is the area of a single GO sheet}$$

From the AFM image of GO sheets, the average lateral width is 0.81 ± 0.13 μm and the corresponding averge area is 0.66 ± 0.2 μm^2. So, K has the value (1.6 ± 0.5) $\times 10^{-4}$ N (0.16 ± 0.05 dyne), which is 5 orders of magnitude higher than that of the smectic LC of small molecules or lipids (10^{-7} dyne), because of the covalently bonded structure of single GO sheet.

Next, we applied Callié line-shape analysis to the first X-scattering peak of the GO liquid crystals with a series of concentrations. Supplementary Figure S13 shows a power-law fitting example in the GO LC with ϕ 2.12%, and we get the value of exponent η as 1.001 with an adjusted R-square of 98.86 %. Referring to the known K, and the $d_{(001)}$ (Supplementary Table S1), we can get the correlation length ξ from equ.1 and equ.2.

With the same analysis procedure, we summarized the correlation length ξ values for GO CLCs with gradient concentrations in Supplementary Table S2.